Polymer Testing 111 (2022) 107612

Contents lists available at ScienceDirect

Polymer Testing

journal homepage: www.elsevier.com/locate/polytest

The effect of different tabbing methods on the damage progression and failure of carbon fiber reinforced composite material under tensile loading

Hafiz Qasim Ali [a,b,c], Çağatay Yilmaz [d], Mehmet Yildiz [a,b,c,*]

[a] Faculty of Engineering and Natural Sciences, Sabanci University, Tuzla, 34956, Istanbul, Turkey
[b] Integrated Manufacturing Tech. Research and Application Center, Sabanci University, Tuzla, 34956, Istanbul, Turkey
[c] Composite Technologies Center of Excellence, Sabanci University-Kordsa, Pendik, 34906, Istanbul, Turkey
[d] Mechanical Engineering, Faculty of Engineering, Abdullah Gul University, Kayseri, Turkey

ARTICLE INFO

Keywords:
Adhesive
Tabbing
Digital image correlation (DIC)
Acoustic emission (AE)
Damage progression

ABSTRACT

Composites are well-known and widely used materials due to their anisotropic nature and high strength-to-weight ratio; therefore, the mechanical performance of these materials is crucial. Precise tensile testing is essential to obtain material properties that are crucial for the design stage of composite structures. This study is an effort to investigate the effect of adhesive materials used for tabbing process, which is necessary for the tensile testing procedure. Araldite and AF 163-2k film are used as the adhesive film, whereas in the case of AF 163-2k, tabbing is done through two different procedures (Jig and corner holes method). Apart from the tensile performance, strain distribution and damage progression are monitored simultaneously using digital image correlation (DIC) and acoustic emission (AE) analysis. It is observed that there is no significant difference in the ultimate tensile strength of these composites tabbed with different adhesives and procedures. Nevertheless, the first major failure strength is much higher in Araldite tabbed specimens compared to AF 163-2k film (the first major failure activity is defined as a point at which material loses its integrity, especially when considering structural or aerospace applications). Also, strain distribution throughout the gauge length recorded via DIC is appreciably different, which is attributed to damage accumulation and progression monitored by AE analysis. The frequency-based analysis of AE data is performed to classify the damage, and cumulative energy is correlated with the DIC to navigate the failure activity at different times and stress levels.

1. Introduction

Carbon fiber-reinforced polymeric composite (CFRP) materials have widespread applications in aerospace, automotive, structural, and defense due to their high strength to weight ratio. The structure's reliability during service is crucial; therefore, different experimental tests are needed to assure the structure's integrity. In composite materials, the strength mainly relies on the stacking sequence of the laminate and is further affected by the manufacturing defects and miss orientation of the fibers [1–3]. The tensile strength of the composite materials is one of the vital deterministic parameters for the mechanical performance of the structure [4]. For the tensile testing of the composite materials, the ASTM D3039 standard is critical, and as per this standard, the test coupons should be tabbed through suitable materials having specified dimensions. Several research works have been conducted to investigate the effect of tabbing on the tensile testing of composite materials.

Winsom et al. [5] showed that the inappropriate load transfer from the tab to the specimen causes premature failure inside the tabbed region of the thin composite sample. To resolve this issue, the use of a tapered tab was proposed in this study. Anane et al. [6] determined the optimal tab design from different tab configurations via finite element analysis and a statistical approach to minimize the stress concentration in a tensile test of non-crimp fiber-based composites. Their results signify that taper angle, tab stiffness, manufacturing process, and adhesive thickness significantly reduce stress concentration. Odom et al. [7] performed compression tests on unidirectional carbon fiber-based epoxy composites. The results suggested that the failure mode is dependent on the tabbing material and the geometry of the tab. Tahir et al. [8] conducted numerical and experimental investigation and proposed a novel tab for tensile testing of unidirectional carbon-reinforced thermoplastic polyamide 6. They found that novel tab design decreases the stress concentration at the tabbed region and

* Corresponding author. Faculty of Engineering and Natural Sciences, Sabanci University, Tuzla, 34956, Istanbul, Turkey
E-mail address: mehmet.yildiz@sabanciuniv.edu (M. Yildiz).

https://doi.org/10.1016/j.polymertesting.2022.107612
Received 26 March 2022; Received in revised form 24 April 2022; Accepted 26 April 2022
Available online 6 May 2022

increases tensile strength by approximately 10%. Belingardi et al. [9] investigated the performance of the E-glass/epoxy fiber-reinforced composite materials under uniaxial loading. Molded and bonded tabs were used to evaluate their significance on the tensile strength. Molded tab considerably reduced the tensile strength of the composite by inducing the stress concentration in the tabbed region; therefore, bonded aluminum tabs were suggested for the better mechanical performance of the composite specimens.

Since tabbing predominantly affects the stress concentration and, in turn, the mechanical performance of the specimen, different instrumental-based approaches have been implemented during the mechanical testing to investigate the damage formation and progression [10–14]. Digital image correlation (DIC) is a non-contact optical method based on the acquisition and tracking of the images based on the stereo sensor system capable of measuring the displacement and then calculating the strain from speckled pattern applied on the surface of the specimen [15,16]. Acoustic emission (AE) analysis can monitor the damage initiation and propagation inside the carbon fiber laminates. Piezoelectric sensors detect the acoustic signals associated with the damage activity and then the AE system classifies them based on their frequency range and amplitude. Caminero et al. [17] studied the damage progression with the help of DIC and X-ray radiography in the notched composite specimen and adhesively bonded patch repaired composite panels under tensile loading. Yilmaz et al. [18] used AE analysis to correlate microdamage and delamination vulnerability of composite materials under tensile loading.

Loutas and Ramirez-Jimenez et al. [19,20] correlated high-frequency acoustic events registered at low strain levels with fiber breakage events. A similar correlation was observed by Gutkin et al. [21]. However, at the ultimate stages of the failure, high-frequency signals were not detected due to the significant release of energy in unidirectional CFRP composites. Several research efforts investigated damage progression in unidirectional CFRP laminates under tension with the help of AE analysis [22–28]. The utilization of a multi-instrumental approach provides a better understanding of the damage mechanism inside the composite materials. Carr et al. [29] combined DIC and AE analysis to correlate the strain measurement with damage location inside the composite material under tensile loading. They observed a relationship between the distribution of the strain and non-uniform damage kinetics. Oz et al. [30] utilized DIC and AE to monitor quasi-isotropic carbon fiber composite laminates under tensile loading and reported that there is a significant difference in the amplitude of the signals which originate from the surface and inner plies of the laminate. Tabrizi et al. [31] conducted a comprehensive and combined numerical and experimental study to investigate the effect of glass and carbon fiber composite-based tabs on the failure analysis of the unidirectional carbon fiber reinforced polymer composites under tensile loading with the help of a multi-instrumental approach such as DIC, AE analysis, and thermography. Their DIC analysis established a relationship between the homogeneity of the strain distribution and tab material. The AE analysis revealed that there are three distinct stages of acoustic emission activities from which the duration of the second stage, which is associated with the interface failure, is significantly affected by the tab material.

There are existing literature studies about the effect of tab materials and grip pressure on the tensile test of composites. Nevertheless, as can be understood from the above-given literature review, only a few studies are dedicated to investigating the effect of adhesive material and the tabbing methodology on the mechanical performance of the carbon fiber-reinforced composite materials subjected to tensile loading. To this end, this study is an unprecedented effort to shed light on the damage progression and failure behavior of different adhesively bonded glass fiber tab-based tensile test coupons with different tabbing methodologies.

This study is a comprehensive effort to investigate the effect of different tabbing adhesives and tabbing procedures on the tensile strength and stress distribution inside the carbon fiber composite coupons. Araldite and AF 163-2 3 M Scotch-weld film are used as adhesive materials to adhere the glass fiber composite-based tabs with carbon fiber composites. Further, two different (jig and corner holes) methods are used to tab the AF 163-2 3M Scotch-weld film. During the tensile test, the in-situ monitoring techniques (DIC and AE) are utilized concurrently, where DIC acquires the strain distribution across the surface of the specimen and AE analysis monitors the damage initiation and propagation inside the laminate.

2. Experimental work

2.1. Materials and sample preparation

In this work, a unidirectional 300 gsm carbon fiber prepreg with a trade code of OM10 T700 12 KT UD300 37% 600 KOMP is used to prepare thin composite laminates. The composite laminates with the dimensions of 320 × 320 mm and a thickness of ∼ 1 mm are manufactured with autoclave curing (ASC Econoclave) in accordance with the recipe recommended by the manufacturer of prepreg which is Kordsa Global. Produced thin composite plates are tabbed with three different tabbing methodologies to investigate the effect tabbing process on the tensile strength and tensile modulus of the carbon fiber composite test sample. Mechanical test specimens are extracted from the tabbed laminates using a robotics-based water jet cutting system with the dimensions stipulated in ASTM D 3039.

2.2. Manufacturing of composite laminate

The lifetime of uncured prepreg at −18 °C is one year; therefore, these prepregs are stored in an industrial fridge. Prepregs were conditioned at +4 °C before cutting, which prevents the water droplet formation on the surface of the prepregs. Uncured unidirectional prepregs were cut into the dimensions of 300 mm × 300 mm with the help of the ZUND G3-L3200 digital ply cutter. The curing mold is initially cleaned with acetone, and then the release agent is coated on the surface before the laying up process. Four layers $[0]_4$ of these prepregs are lay-up on top of each other to maintain the cured thickness of 1 mm. The stacked prepreg lay-up on the mold and then covered with peel ply and breather layers. After that, the whole configuration is confined using a single sheet vacuum bag and left under vacuum for 30 min for the debulking process. The curing of the prepreg was carried out in ASC autoclave using the curing cycle recommended by the manufacturer of the prepreg. A full vacuum (1 bar) is initially applied, followed by the 7-bar gauge autoclave pressure. After that, when the autoclave pressure reaches 1 bar, the vacuum is reduced to a safety value of 0.2 bar. The heating is applied at a ramp rate of 3 °C/min up to 120 °C and then holds for 60 min, which is followed by a cooling down to 60 °C at a rate of 3 °C/min.

2.3. Tabbing with jig

A layer of AF 163-2k red adhesive film purchased from 3 M Company is adhered between the CFRP laminate and glass fiber composite tab. A similar procedure is repeated to tab all the sides of the carbon fiber laminate. Then, the carbon fiber laminate with glass tabs on all sides is placed on a jig fixture shown in Fig. 1. The proper alignment of this tabbing setup is ensured with the help of fixed pins. The pins not only guarantee the alignment of glass fiber tabs over the surface of carbon fiber laminate but also maintain the gauge length of 150 mm required for tensile testing according to the ASTM D-3039. After the alignment inspection, the whole setup is bagged for curing. The bagging procedure comprises three stages where initially, the lay-up is covered with one layer of non-perforated release film (Airtech Wrightlon 5200). Second, a breather fabric (Airtech N10) is placed to ensure a homogeneous airflow over the lay-up. Release film prevents the sticking of breather fabric to

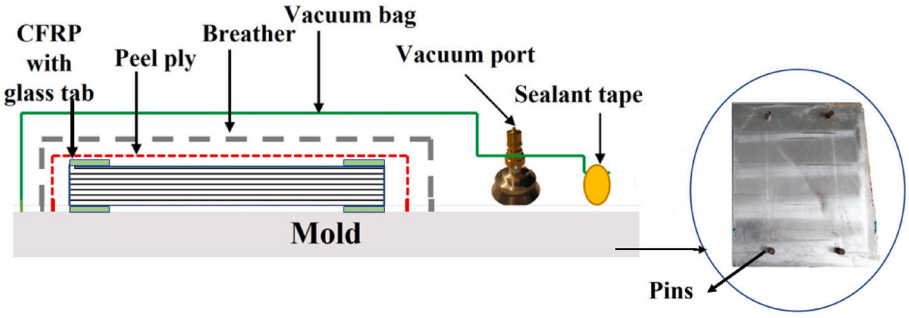

Fig. 1. Tabbing fixture for jig and bagging configuration.

the adhesive film. Finally, the whole setup is covered with a vacuum bag (Airtech Wrightlon 7400), and the vacuum bag is sealed with the help of Airtech AT 200Y vacuum tape (Fig. 1). Before the sealing, an N-type thermocouple is placed inside the setup in such a way that it touches the AF 163-2k red adhesive film. Then bagged setup is tested for a vacuum leak for 10 min and then placed in an industrial oven (Sistem Teknik industrial furnace).

2.4. Tabbing with corner holes

The tabbing process is carried out through drilling holes on the corner of the glass fiber composite tab material and CFRP laminate. AF 163-2k red adhesive film is attached to the glass fiber composite tabs, and then these tabs are then fixed to the CFRP laminate by inserting metal pins inside the drilled holes, as shown in Fig. 2. Apart from the usage of the jig, a similar procedure defined in the above section is used for the bagging process. Tabbing with the corner holes method has two significant advantages compared to the one with the jig. First, both sides of the test sample can be heated homogeneously. When tabbing jig is used, one side of the CFRP laminate is in contact with the metal jig that is made of aluminum. The vacuum bagging is carried out on the other side of the laminate, which is not covered with metal (Fig. 1). The side where the laminate is covered with a vacuum bag reaches the desired temperature earlier as compared to the other side. This difference between the contact surfaces creates a temperature gradient on both sides of the laminate. In the case of the corner hole tabbing method, both sides of the laminate are covered with the vacuum bag (enveloped/sandwiched by the bagging configuration); therefore, heat distribution is uniform on both sides.

Second, the CFRP laminate has glass tabs on both sides; therefore, it is not in direct contact with the mold surface. Since the jig tabbing setup is covered with the vacuum bagging configuration on the other side, which applies a bending load on the laminate due to vacuum pressure that causes deformation and residual stresses formation inside the CFRP laminate during the adhesive curing procedure.

2.5. Curing of adhesive film

The adhesive film is cured by following the recommendations of the manufacturer, which includes the following stages. The temperature of the bagged setup is increased up to 125 °C with a ramp of 3 °C/min. kept at this temperature for 70 min followed by a temperature drop down till 75 °C. The gage vacuum is kept constant at around −270 mbar (Fig. 3b) during the whole curing cycle. The “Air Tc actual” is the actual air temperature inside the oven which is measured by a thermocouple. While “Air Tc set” is the desired value of the air temperature inside the oven, which is set during the programming of the oven. It can be observed that the temperature inside the oven measured by a thermocouple follows the path of the temperature set inside the oven software (Fig. 3a). It can be seen from Fig. 3b that there is no leakage of the vacuum during the whole curing process.

2.6. Tabbing with araldite

Araldite 2011, a two-component epoxy adhesive, has been extensively used for the tabbing of composite materials due to its high lap shear strength (11.30 MPa) for glass fiber reinforced composites and high shear modulus (1.2 GPa), and room temperature curing. For tabbing process, the surface of both specimen and tabs are slightly roughened with 320-grade emery paper and then rinsed with ethanol. A thin layer of Araldite adhesive is applied between tab and specimen, a weight of 5 N is exerted (Fig. 4) on the tab to improve the adhesion therein, and the composite plate/tab setup is then allowed to cure for 24 h before the test.

2.7. Mechanical testing

The tensile test is performed as per the ASTM D3039 standard. According to the standard, the dimensions of the tabbed region are 50 mm × 15 mm. Eight specimens from each batch were cut according to the desired gauge length, width and thickness of 250 mm, 15 mm, and 1

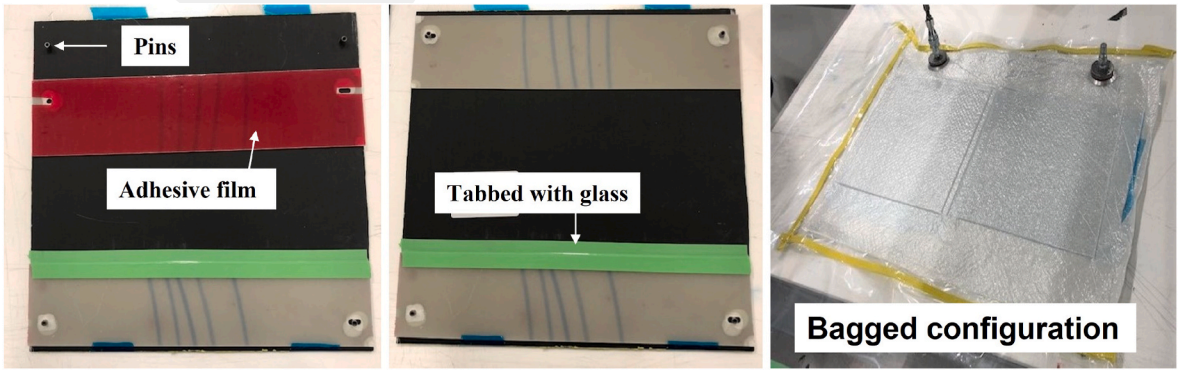

Fig. 2. Schematic representation of tabbing with corner holes method.

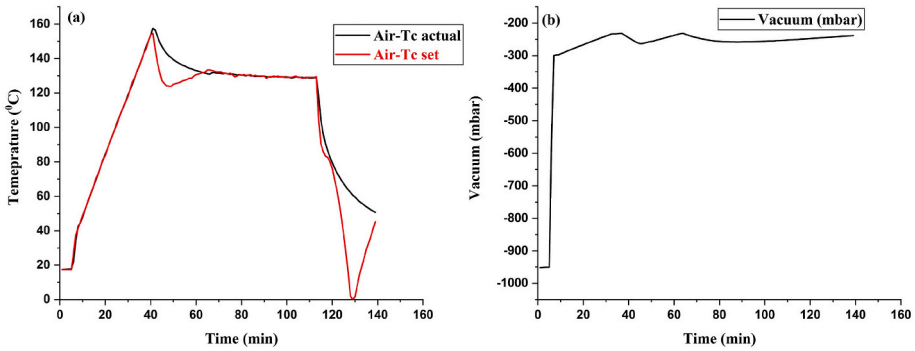

Fig. 3. (a) Temperature & (b) vacuum profile for curing of adhesive film.

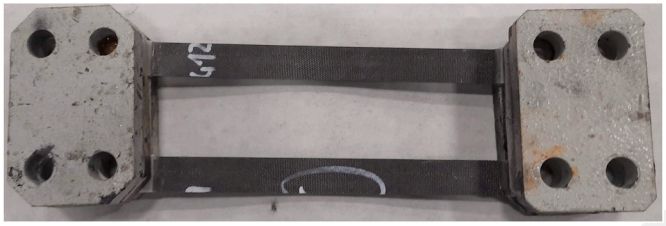

Fig. 4. Tabbing with Araldite.

mm, respectively, through a water jet cutting system. The nomenclature for three specimen batches, namely, AF 163-2k tabbing with a jig, AF 163-2k tabbing with corner holes and tabbing with Araldite adhesive is J, D, and AR, respectively.

For each specimen batch, a speckle pattern is created through black and white paint for full-field strain measurement using a digital image correlation (DIC) system (GOM 12 M sensor-based stereo system). The 3D calibration is performed as per the instructions for the 250 × 200 calibration object. The working distance is 1250 mm, and the camera angle is 25^o. The obtained calibration results are in the ideal range where calibration deviation is 0.036 pixels (OK limit: 0.050) and scale deviation value is 0.002 mm (OK limit: 0.022 mm). For the post-processing, ARAMIS professional software is used where facet and step size values are 24 and 19 pixels, respectively. A schematic of the experimental setup is shown in Fig. 5.

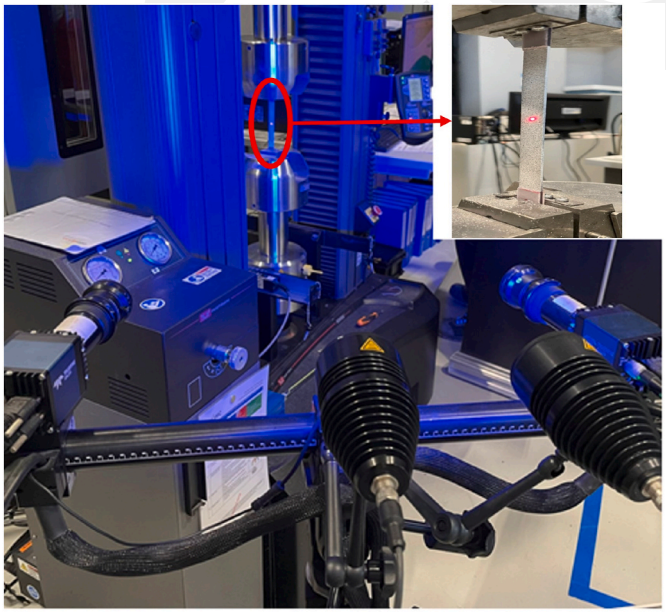

Fig. 5. Experimental test setup.

Acoustic emission (AE) analysis is performed using Mistras PCI-2AE equipment, where wideband piezoelectric sensors (PICO 200–750 kHz) are used for the data acquisition. Two sensors with a gap of 60mm between them are adhered to the surface of the specimen within its gauge length by employing a hot silicon gun (Fig. 6). A 20dB gain via a physical acoustic 0/2/4 voltage preamplifier amplifies the acoustic signals tenfold, which are received from micro-damage events inside the material. The desired hardware parameters are chosen on the AEwin PCI2-4 software for the analysis, which are set to a threshold of 50 dB, peak definition time of 50 μs, hit definition time of 150 μs, hit lock time of 300 μs, and a sampling rate of 2 mega samples per second. The extracted data are filtered using a Bessel bandpass filter of 20–800 kHz through Noesis 7 software. Then, weighted peak frequency (WPF) is calculated by using peak frequency and frequency centroid features [32]. Then, the MATLAB® programming platform is used to cluster the data and to plot WPF against partial power 2 (PP2), which is extracted through Fast Fourier Transformation $\bar{U}(f)$ of the signals and calculated using eq (1). Silhouette coefficient and Davies-Bouldin index criteria are used to predict the optimal number of clusters, and then the K-means method is used for clustering the data.[33]

$$Partial\ power = \frac{\left(\int_{f_1}^{f_2} \overline{U}^2(f)df\right)}{\int_{0kHz}^{1200kHz} \overline{U}^2(f)df} \quad (1)$$

$$Partial\ power\ (PP2)\ range\ : f_1 = 250kHz\ and\ f_2\ = 450kHz$$

3. Results and discussions

Five specimens of each batch are tested as per ASTM D3039, where damage progression is monitored through AE while full-field strain measurement is performed via DIC. Average stress values and their standard deviations and maximum stress values for each batch are listed in Table 1.

It can be observed from Table 1 that there is no significant difference in the stress values of these batches. AR has the highest average stress value, and its standard deviation is also lower. Almost all the specimens from each batch show a similar full-field strain pattern and damage activities concerning their batch; therefore, one specimen from each batch whose value is close to the average stress value of the given batch is chosen as a representative specimen to understand the effect of tabbing adhesive on the failure of the composite material. The code names and maximum stress values of the representative specimens are given as follows, JR (2260.7 MPa), DR (2323 MPa), and ARR (2334.2 MPa).

3.1. Digital image correlation

The full-field strain map of each specimen is recorded through a stereo 3D-DIC system. This measurement system is advantageous as it

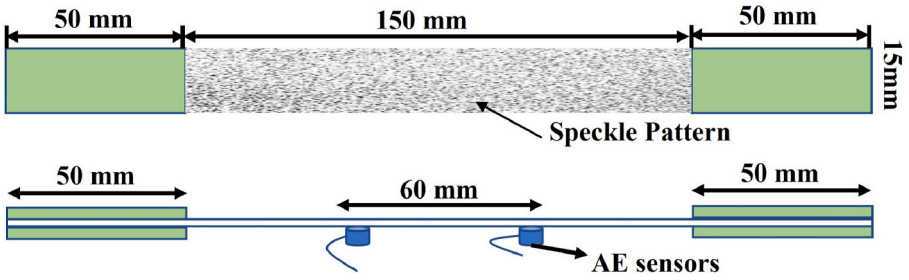

Fig. 6. Dimensions of the specimen along with AE sensors position.

Table 1
Tensile testing results of all the specimens.

Nomenclature Average Stress (AS) (MPa)
J 2291.4
D 2310.9
AR 2321.6
Standard Deviation for AS (MPa) Maximum Stress (MS) (MPa)
87.3 2395.7
101.5 2467.6
82.5 2439.9

provides information regarding local strain variations if there is any heterogeneity due to uneven stress distribution caused by the crack formation and/or residual stresses originating during cutting and tabbing processes. A speckle pattern is created over the whole gauge length of the representative samples (JR, DR, ARR). Fig. 7 shows the stress-strain curves of the representative specimens, and from these curves, it can be observed that there is no significant difference between the specimens' ultimate stress and strain values. Until the mid-stress value (~1200 MPa), the stress-strain curves are uniform, and there is no significant aberration in the strain values. The inset in Fig. 7 corresponds to the stress range of 1500–2000 MPa, from which one can observe that the DR specimen shows a significant aberration on the curve caused by the damage activities while JR has the lowest one. Moreover, ARR shows a much smoother stress-strain curve than the other two specimens until 1900 MPa. The aberrations occur due to the damage formation to be elaborated on in the forthcoming parts.

In the case of unidirectional fiber-based composites, DIC can enable a reliable prediction of stress-concentrated regions even at lower load levels [31] It can be seen from Fig. 8 that both JR and DR samples have

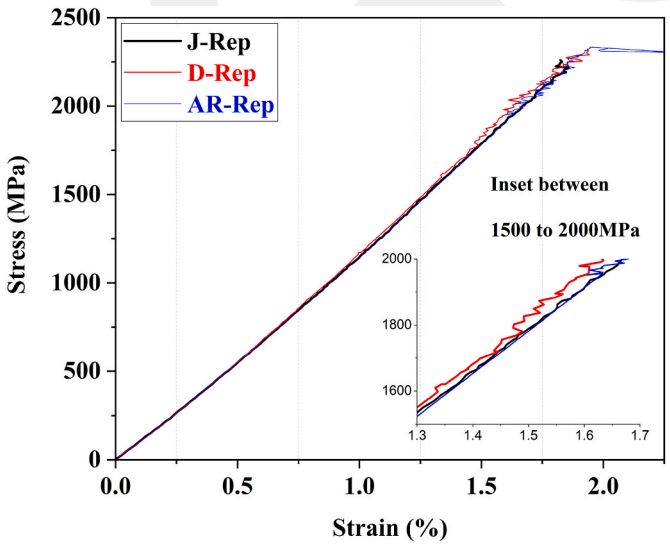

Fig. 7. Stress-strain curves of representative specimens.

high strain regions at the edges within the gauge length of the specimens. In contrast, ARR has a heterogeneous strain across the gauge length of the specimen. One of the key factors for the presence of stress concentration regions is the machining of the specimens, which promotes micro damages at the edges of the specimen that may potentially lead to the formation of macro damages. In a unidirectional laminate, these micro damages located at the edges can cause splitting of plies, whereas, in woven composites, these cracks can propagate along the 90° fibers. Fig. 8 (a) & (b) shows that stress in the case of JR and DR is concentrated at the edges instead of being distributed across the gauge length, whereas ARR has stressed regions across the whole gauge length, which might be due to the effect of adhesive used for the tabbing. In the case of JR and DR specimens, recall that AF 163-2k is used, which is a thick (0.25 mm) film-based adhesive. Given the fact that the entire bonding assembly is composed of non-conducting materials, the applied heat for curing does not transfer properly to the adhesive during the tabbing procedure, which might cause some void formation or uncured regions within the adhesive film. Consequently, uneven stress distribution will be unavoidable and, in turn, promote splitting in the plies, resulting in damage initiations at the lower loading level. Moreover, the CFRP laminate is exposed to the second heating cycle for curing of tabbing adhesive, which may cause thermal distortion and residual stress formation inside the laminate. Contrarily, as for the ARR specimen tabbed with Araldite bi-component epoxy-based adhesive, the void formation can be avoided relatively easily by applying pressure during the tabbing process. Fig. 8a compares the strain distribution across the gauge length of all the representative specimens. Specimen JR has a high strain concentration at the left edge, most probably due to micro-damage formation during machining, whereas DR has strain concentration at the upper left edge in addition to some local non-uniform strain distribution across the gauge length. However, in the ARR specimen, the strain is heterogeneous across the whole gauge length, even at 1000 MPa, which might be due to the occurrence of micro damages in the transverse direction [31]. In JR, DR and ARR specimens, the first minor visible edge splitting occurs at 1055. MPa, 968 MPa and 1476 MPa, respectively. Fig. 8b presents strain distribution for JR, DR and ARR specimens with their corresponding stress levels of 1055 MPa, 968 MPa, and 1476 MPa, respectively, at which the first major failure is about to take place. The first major splitting failure is defined as the stress level at which the failure is predominantly visible and is a critical attribute of the composite material for structural or aerospace applications since the material loses its integrity extensively. Specimen JR at 1405 MPa shows higher strain distribution near the bottom grip and across the left edge where minor splitting happened earlier. Sample DR at 1590 MPa experiences higher strain levels near the top and bottom region and around the left edge of the gauge length, while the ARR at 1950 MPa has a higher strain concentration at the left edge where minor splitting has happened earlier, and the damage growth progresses in the transverse direction. Fig. 8c exhibits the strain distribution for all representative specimen configurations where the first major splitting has just occurred at the stress levels of 1410 MPa, 1591 MPa and 1951 MPa for JR, DR, and ARR in the given order. Here it can be depicted that the magnitude of the failure is much more

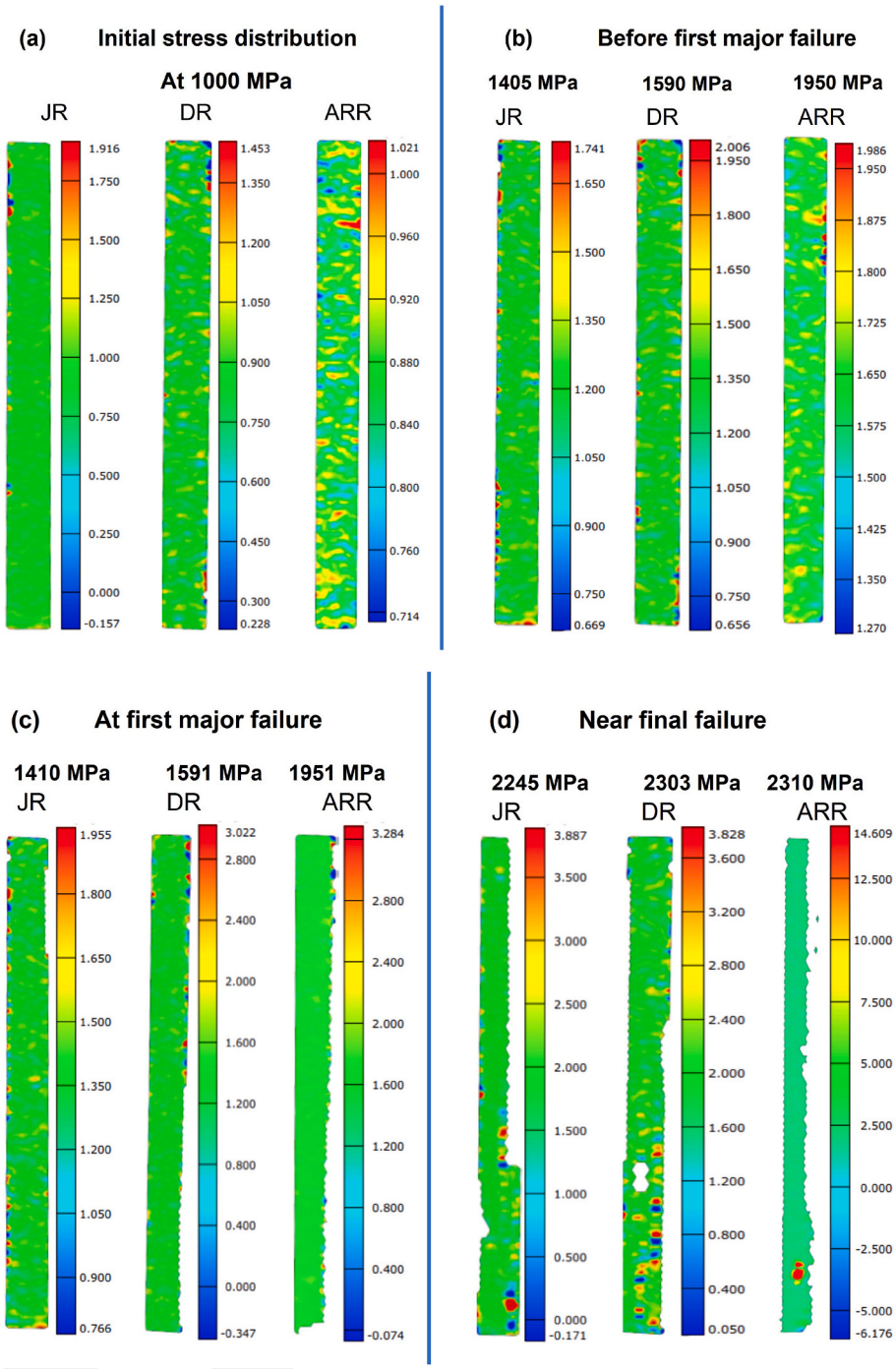

Fig. 8. Strain maps of representative specimens, (a) At 1000 MPa, (b) Just before first major failure, (c) At first major failure, (d) Near final failure.

significant in the ARR specimen, but it happened at a higher stress level than DR and JR. Fig. 8d presents the strain distribution near the final failure strength, and here it can be seen that the material is not capable of withstanding further loading, and final failure will be a global failure. Although there is not much significant difference in the ultimate final strength of these composite specimens, there is a significant difference in the first major failure strength.

3.2. Acoustic emission (AE)

In acoustic emission analysis, different parameters have been used extensively to characterize damage accumulation and progression. Most of the studies [36–39] used amplitude and peak frequency as parameters to classify the damage. Although frequency-based parameters are reliable, as shown in many studies, the issue with the amplitude is that it is highly dependent on the location of the damage. If the activity occurs near a sensor or the surface of the specimen, it results in high amplitude, whereas the amplitude will be lower if the damage occurs inside the plies or far away from the sensor location [37–40]. There are some contradictions for the reliability of amplitude in the literature [21,29,30,32–35] due to the damage dependency on the material type and loading configuration.

Unidirectional CFRP laminates tabbed with different adhesives were tested under tension, and acoustic emission data was simultaneously recorded at a sampling rate of 2 MSPS. Mentioned in the above section, the small aberrations in the stress-strain curve, specifically at low

loading levels, can be attributed to the microdamage activities such as matrix cracking (MC) and damage formation at the edges of the specimen, which might have been caused by water jet-based specimen cutting process. As the tests proceed, the aberration increases due to the surge in damage activities such as splitting, which is predominantly caused by interface failure (IF) and fiber failure (FF). In the case of a unidirectional laminate, AE sensors cannot record the high-frequency failure owing to extensive splitting caused by high energy release at the ultimate stages of failure, which causes sensor detachment from the surface of the specimen [21].

The most prominent parameters obtained from acoustic emission analysis are amplitude, counts, energy, and frequency. In Fig. 9(a–c), different parameters obtained from the acoustic emission analysis are plotted for each representative specimen (JR, DR, and ARR) to observe their efficacy for damage detection. The selected parameters for the analysis are energy, signal strength, counts, and RA value (defined as the rise time divided by amplitude). The cumulative curves of these parameters are plotted against the stress-strain curve to compare their reliability. It can be seen in Fig. 9 that the cumulative counts and cumulative RA value curves show the trend of logistic growth and do not provide any significant evidence about damage activities apart from some major events. In contrast, cumulative energy and cumulative signal strength curves show step-growth, and each step refers to a damage incident inside the material, which can also be observed in the inset DIC images at some significant steps in the cumulative energy curve. Therefore, signal strength or energy can be chosen to classify the damage activities further.

Weighted peak frequency (WPF) is defined as the square root of peak frequency and frequency centroid product. It is one of the most adaptive frequency parameters to classify the damage type in composite materials and has been used extensively in the literature [10,18,30,34,35]. Herein, WPF and partial power 2 (PP2) features of acoustic emission analysis are used for the damage classification. K-means clustering algorithm with Euclidean distance function is utilized for the clustering where the number of clusters (k) is decided based on Silhouette coefficient (SC) and Davies-Bouldin index (DB). The value of SC ranges between 0 and 1, where scores are higher for the dense and well-distributed clusters, while the DB index relates to the cluster centroids, and it is the ratio of the distance within the cluster and the distance between these clusters. The optimal k value from both criteria is the one that has a higher SC coefficient and low DB index [42], which is three in the case of all the representative specimens, i.e., JR, DR, and ARR, as can be seen in Fig. 10.

The results of the classification of the representative specimen after implementing the k-means algorithm are illustrated in Fig. 11(a–c). Three identified major failure types ranging from low-to high-frequency are respectively named matrix cracking (MC), Interface failure (IF), and fiber failure (FF). The percentages of failure types classified via K-means clustering analysis are shown in Fig. 12. Since the specimen contains unidirectional fibers, the major failure type is a fiber failure, which is 55.85, 49.6%, and 53.8% in JR, DR, and ARR specimens, respectively. In DR and ARR specimens, the interface failure is higher than the matrix failure that causes extensive splitting, which reveals itself as an aberration in the stress-strain curve, particularly at elevated stress levels, and can be seen in their respective stress-strain curves. Specimen JR has the highest percentage of matrix failure, and its stress-strain curve (Fig. 7) is smoother than DR and ARR specimens.

The damage development and progression mechanisms are complex in composite materials due to their anisotropic nature. Furthermore, in the case of UD laminates, which are bereft of reinforcing fibers in the transverse direction, any minuscule damages inflicted at the edges of the specimens by water jet based or other cutting processes, which are rather random and unavoidable, may cause stress concentration regions. The regions with high-stress concentrations are prone to matrix cracking and complex damage formation that can cause debonding and fiber breakage. Fig. 13a-c exhibits the cumulative energy along the stress-strain curve due to damage accumulation in specimens together with corresponding inset DIC images. As can be seen from Fig. 13. all the

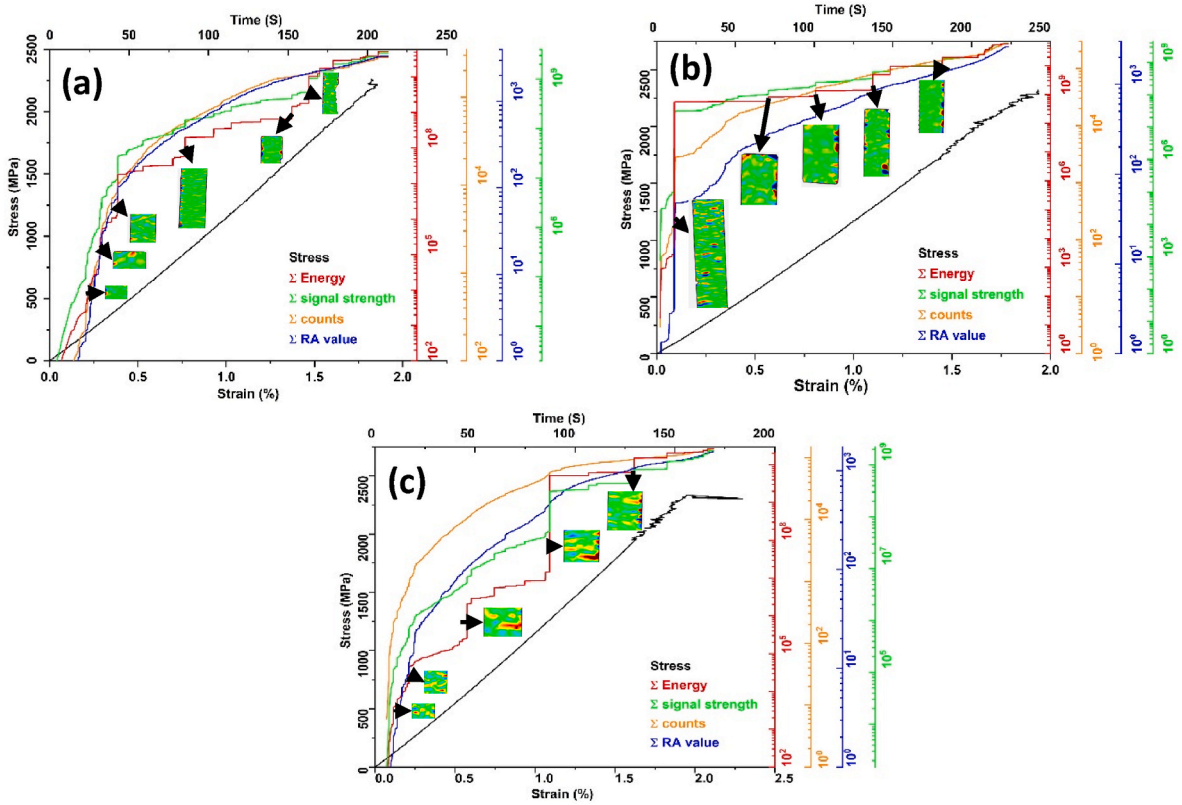

Fig. 9. Comparison of different AE parameters for representative samples (a) JR, (b) DR, and (c) ARR.

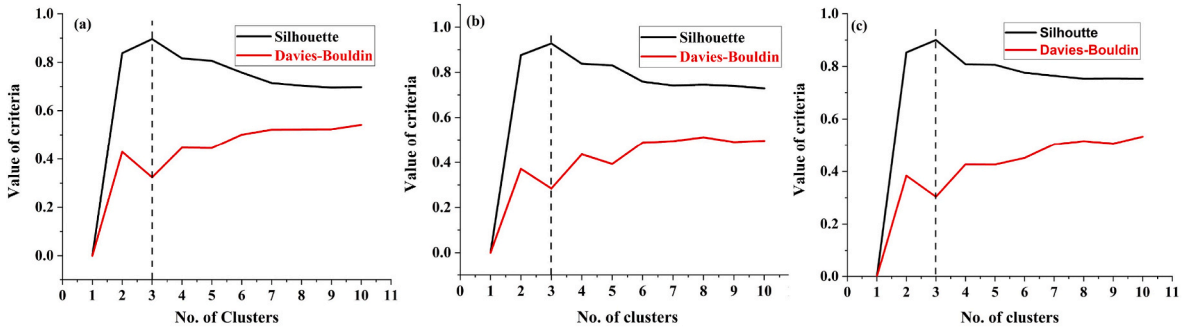

Fig. 10. Estimation of the number of clusters through Silhouette coefficient and Davies-Bouldin index for (a) JR, (b) DR, and (c) ARR.

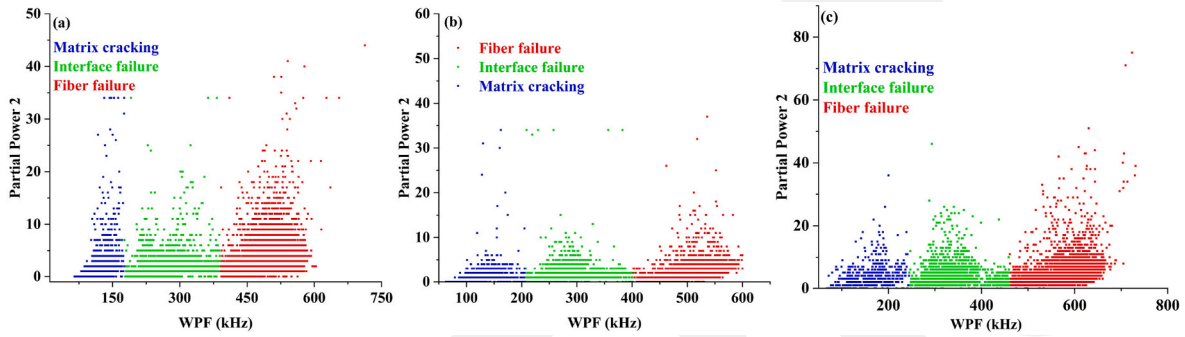

Fig. 11. Clustering results for (a) JR, (b) DR and (c) ARR.

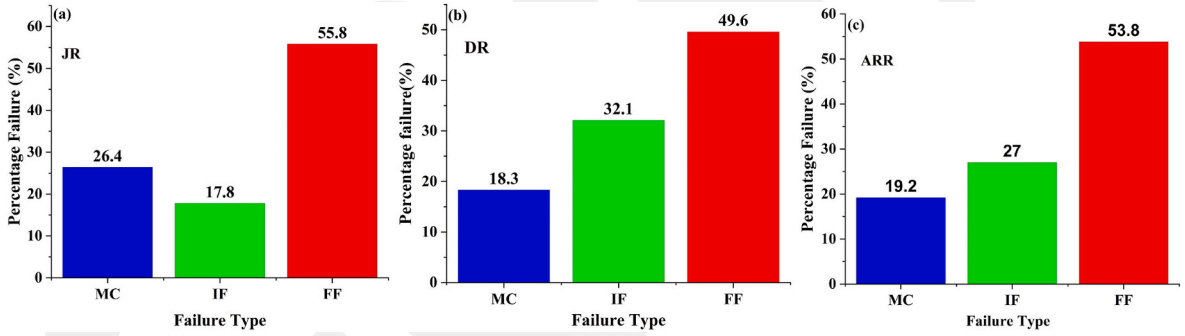

Fig. 12. Percentage of different failure types in (a) JR, (b) DR, and (c) ARR.

damage activities start simultaneously at a lower load level, indicating that they are associated with each other and significantly contribute to damage progression, thus leading to final failure. In the case of JR and DR (Fig. 13 (a) and (b)), initial failure activities occur across the gauge length. However, as the test proceeds, there is significant step formation in all kinds of failure types in JR and DR. The DIC thumbnails show that most of these activities are associated with the damage progression near the edges where splitting occurs at higher load levels. Nevertheless, in the case of ARR (Fig. 13c), there are a substantial number of steps in all types of damage, especially in MC and IF-based failures. The DIC pattern shows that around 1500 MPa stress level, the damage activities are observed everywhere inside the gauge length of the specimen. However, after the stress level of 1500 MPa, there is a considerable damage progression at the edge, which already had a stress concentration region. The failure in this region initiates around 900 MPa and then propagates until 1500 MPa and then causes the global failure.

4. Conclusion

Composites are anisotropic materials that make their damage mechanism more complex. This study aims to understand the effect of tabbing adhesive and procedure on the mechanical performance and failure mechanisms of composite materials under tensile loading. The tensile specimens are tabbed using two different adhesive systems named Araldite and AF 163-2k, where two different manufacturing methods are employed for tabbing through AF 163-2k adhesive film. It is noticed that there is no significant difference in the ultimate tensile strength of the material; therefore, if the final strength is concerned during the application, then an inexpensive material, like Araldite, can be used instead of AF 163-2k. However, in the case of aerospace and high-performance-based applications, the first major failure activity strength is critical as the material loses its integrity at this failure point. Araldite tabbed specimen (ARR) performs better than AF 163-2k-based adhesive-based specimens (JR and DR), which is depicted by digital image correlation analysis.

Furthermore, damage mechanisms are scrutinized through acoustic emission analysis, where several parameters are initially compared to each other to check their applicability for understanding damage progression. Both energy and signal strength are the most reliable parameters and correlate well with the digital image correlation analysis. After

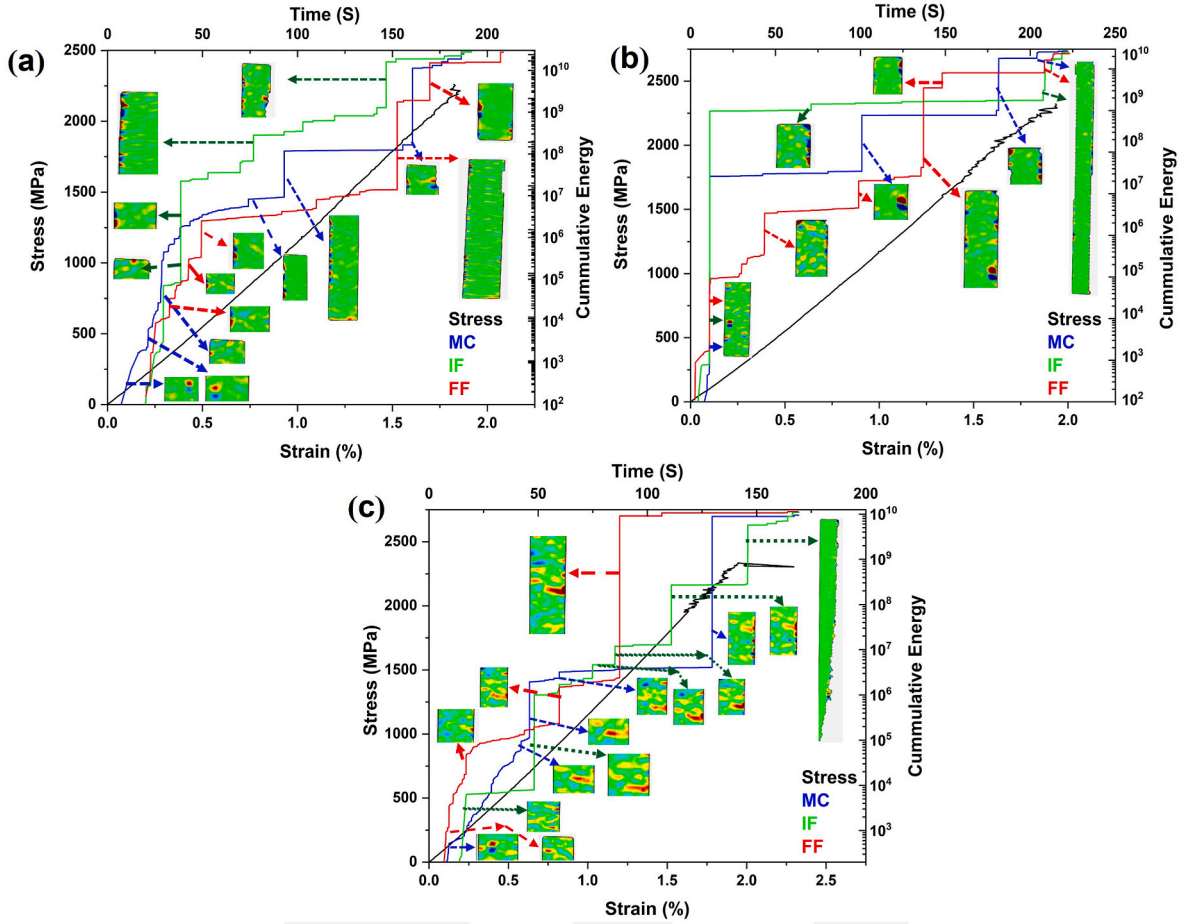

Fig. 13. Cumulative energy and stress-strain curve for representative specimens (a) JR (b) DR, and (c) ARR.

that, weighted peak frequency (WPF) and partial power 2 (PP2) are used for clustering to classify the types of damage in representative specimens. The damage activities are classified as matrix cracking, interface failure and fiber failure, and it is found that the most predominant failure type in all the specimens is fiber failure. In the case of the DR specimen, the interface-based failure is higher, and it causes extensive splitting inside the specimen, resulting in the aberration in the stress-strain curve. Moreover, the cumulative energy of these failure types is plotted against the stress-strain level for all the representative specimens. It can be observed that step formation in these cumulative energy curves is caused by damage activities which are also detected by the digital image correlation analysis.

5. Data availability

The raw data used to produce these findings are available from the corresponding author upon reasonable request.

CRediT authorship contribution statement

Hafiz Qasim Ali: Conceptualization, Methodology, Testing, Formal analysis, Writing – review & editingWriting -reviewing & editing. **Çağatay Yilmaz:** Conceptualization, Manufacturing, Writing – review & editingWriting – review &amp editing. **Mehmet Yildiz:** : Writing — review & editingWriting – review & editing, Supervision, Project administration.

Declaration of competing interest

The authors declare that they have no known competing financial interests or personal relationships that could have appeared to influence the work reported in this paper.

Acknowledgment

The authors would like to acknowledge the partial support from Sabancı University Integrated Manufacturing Technologies Research And Application Center.

References

[1] R.M.A. Khan, I.E. Tabrizi, H.Q. Ali, E. Demir, M. Yildiz, Investigation on interlaminar delamination tendency of multidirectional carbon fiber composites, Polym. Test. 90 (2020), https://doi.org/10.1016/j.polymertesting.2020.106653.
[2] H.Q. Ali, I.E. Tabrizi, R.M. Awais Khan, J. Seyyed Monfared Zanjani, C. Yilmaz, L. H. Poudeh, et al., Experimental study on dynamic behavior of woven carbon fabric laminates using in-house piezoelectric sensors, Smart Mater. Struct. 28 (2019), https://doi.org/10.1088/1361-665X/ab34f3.
[3] Z.-M. Huang, Y.-X. Zhou, Strength of Multidirectional Laminates. Strength of Fibrous Composites, Springer, 2011, pp. 145–235.
[4] Tabbing Guide for Composite Test Specimens n.D. (accessed March 23, 2022), https://apps.dtic.mil/sti/citations/ADA411472.
[5] M.R. Wisnom, B. Khan, S.R. Hallett, Size effects in unnotched tensile strength of unidirectional and quasi-isotropic carbon/epoxy composites, Compos. Struct. 84 (2008) 21–28.
[6] K. Anane-Fenin, E.T. Akinlabi, N. Perry, A numerical and statistical approach for optimization of tab design for non-crimp fabric composites, Procedia Manuf. 35 (2019) 820–825, https://doi.org/10.1016/j.promfg.2019.06.027.
[7] E.M. Odom, D.F. Adams, Failure modes of unidirectional carbon/epoxy composite compression specimens, Composites 21 (1990) 289–296, https://doi.org/10.1016/0010-4361(90)90343-U.

[8] M.M. Tahir, W.-X. Wang, T. Matsubara, A novel tab for tensile testing of unidirectional thermoplastic composites, J. Thermoplast. Compos. Mater. 32 (2017) 37–51, https://doi.org/10.1177/0892705717743295.

[9] G. Belingardi, D.S. Paolino, E.G. Koricho, Investigation of influence of tab types on tensile strength of E-glass/epoxy fiber reinforced composite materials, Procedia Eng. 10 (2011) 3279–3284, https://doi.org/10.1016/j.proeng.2011.04.541.

[10] H.Q. Ali, I. Emami Tabrizi, R.M.A. Khan, A. Tufani, M. Yildiz, Microscopic analysis of failure in woven carbon fabric laminates coupled with digital image correlation and acoustic emission, Compos. Struct. 230 (2019) 111515, https://doi.org/10.1016/j.compstruct.2019.111515.

[11] R.M.A. Khan, S. Saeidiharzand, I. Emami Tabrizi, H.Q. Ali, M. Yildiz, A novel hybrid damage monitoring approach to understand the correlation between size effect and failure behavior of twill CFRP laminates, Compos. Struct. 270 (2021) 114064, https://doi.org/10.1016/j.compstruct.2021.114064.

[12] A. Sendrowicz, A.O. Myhre, S.W. Wierdak, A. Vinogradov, Challenges and accomplishments in mechanical testing instrumented by in situ techniques: infrared thermography, digital image correlation, and acoustic emission, Appl. Sci. 11 (2021) 6718.

[13] A. Ichenihi, W. Li, Y. Gao, Y. Rao, Feature selection and clustering of damage for pseudo-ductile unidirectional carbon/glass hybrid composite using acoustic emission, Appl. Acoust. 182 (2021) 108184, https://doi.org/10.1016/j.apacoust.2021.108184.

[14] N. Feito, J.V. Calvo, R. Belda, E. Giner, An experimental and numerical investigation to characterize an aerospace composite material with open-hole using non-destructive techniques, Sensors 20 (2020), https://doi.org/10.3390/s20154148.

[15] Digital Image Correlation and Tracking - Wikipedia n.D. https://en.wikipedia.org/wiki/Digital_image_correlation_and_tracking. (Accessed 28 September 2021) accessed.

[16] J. Carr, J. Baqersad, C. Niezrecki, P. Avitabile, M. Slattery, Dynamic stress-strain on turbine blade using digital image correlation techniques Part 1: static load and calibration, Conference Proceedings of the Society for Experimental Mechanics Series 2 (2012) 215–220, https://doi.org/10.1007/978-1-4614-2422-2_20.

[17] M.A. Caminero, M. Lopez-Pedrosa, C. Pinna, C. Soutis, Damage monitoring and analysis of composite laminates with an open hole and adhesively bonded repairs using digital image correlation, Compos. B Eng. 53 (2013) 76–91, https://doi.org/10.1016/j.compositesb.2013.04.050.

[18] C. Yilmaz, M. Yildiz, A study on correlating reduction in Poisson's ratio with transverse crack and delamination through acoustic emission signals, Polym. Test. 63 (2017) 47–53, https://doi.org/10.1016/j.polymertesting.2017.08.001.

[19] T.H. Loutas, V. Kostopoulos, C. Ramirez-Jimenez, M. Pharaoh, Damage evolution in center-holed glass/polyester composites under quasi-static loading using time/frequency analysis of acoustic emission monitored waveforms, Compos. Sci. Technol. 66 (2006) 1366–1375, https://doi.org/10.1016/J.COMPSCITECH.2005.09.011.

[20] C.R. Ramirez-Jimenez, N. Papadakis, N. Reynolds, T.H. Gan, P. Purnell, M. Pharaoh, Identification of failure modes in glass/polypropylene composites by means of the primary frequency content of the acoustic emission event, Compos. Sci. Technol. 64 (2004) 1819–1827, https://doi.org/10.1016/J.COMPSCITECH.2004.01.008.

[21] R. Gutkin, C.J. Green, S. Vangrattanachai, S.T. Pinho, P. Robinson, P.T. Curtis, On acoustic emission for failure investigation in CFRP: pattern recognition and peak frequency analyses, Mech. Syst. Signal Process. 25 (2011) 1393–1407, https://doi.org/10.1016/J.YMSSP.2010.11.014.

[22] P.J. de Groot, P.A.M. Wijnen, R.B.F. Janssen, Real-time frequency determination of acoustic emission for different fracture mechanisms in carbon/epoxy composites, Compos. Sci. Technol. 55 (1995) 405–412, https://doi.org/10.1016/0266-3538(95)00121-2.

[23] C.R. Ramirez-Jimenez, N. Papadakis, N. Reynolds, T.H. Gan, P. Purnell, M. Pharaoh, Identification of failure modes in glass/polypropylene composites by means of the primary frequency content of the acoustic emission event, Compos. Sci. Technol. 64 (2004) 1819–1827, https://doi.org/10.1016/J.COMPSCITECH.2004.01.008.

[24] T.H. Loutas, V. Kostopoulos, C. Ramirez-Jimenez, M. Pharaoh, Damage evolution in center-holed glass/polyester composites under quasi-static loading using time/frequency analysis of acoustic emission monitored waveforms, Compos. Sci. Technol. 66 (2006) 1366–1375, https://doi.org/10.1016/J.COMPSCITECH.2005.09.011.

[25] R. Gutkin, C.J. Green, S. Vangrattanachai, S.T. Pinho, P. Robinson, P.T. Curtis, On acoustic emission for failure investigation in CFRP: pattern recognition and peak frequency analyses, Mech. Syst. Signal Process. 25 (2011) 1393–1407, https://doi.org/10.1016/J.YMSSP.2010.11.014.

[26] T. Prieß, M.G.R. Sause, D. Fischer, P. Middendorf, Http://DxDoiOrg/101177/0021998314552003, Detection of Delamination Onset in Laser-Cut Carbon Fiber Transverse Crack Tension Specimens Using Acoustic Emission, vol. 49, 2014, p. 2639, https://doi.org/10.1177/0021998314552003, 47.

[27] M. Fotouhi, P. Suwarta, M. Jalalvand, G. Czel, M.R. Wisnom, Detection of fibre fracture and ply fragmentation in thin-ply UD carbon/glass hybrid laminates using acoustic emission, Compos. Appl. Sci. Manuf. 86 (2016) 66–76, https://doi.org/10.1016/J.COMPOSITESA.2016.04.003.

[28] R. Mohammadi, M.A. Najafabadi, M. Saeedifar, J. Yousefi, G. Minak, Correlation of acoustic emission with finite element predicted damages in open-hole tensile laminated composites, Compos. B Eng. 108 (2017) 427–435, https://doi.org/10.1016/J.COMPOSITESB.2016.09.101.

[29] C. Flament, M. Salvia, B. Berthel, G. Crosland, Local Strain and Damage Measurements on a Composite with Digital Image Correlation and Acoustic Emission, vol. 50, 1989, https://doi.org/10.1177/0021998315597993, 96.

[30] F.E. Oz, N. Ersoy, M. Mehdikhani, S v Lomov, Multi-instrument in-situ damage monitoring in quasi-isotropic CFRP laminates under tension, Compos. Struct. 196 (2018) 163–180, https://doi.org/10.1016/j.compstruct.2018.05.006.

[31] I.E. Tabrizi, R.M.A. Khan, E. Massarwa, J.S.M. Zanjani, H.Q. Ali, E. Demir, et al., Determining tab material for tensile test of CFRP laminates with combined usage of digital image correlation and acoustic emission techniques, Compos. Appl. Sci. Manuf. 127 (2019), https://doi.org/10.1016/j.compositesa.2019.105623.

[32] C. Yilmaz, C. Akalin, I. Gunal, H. Celik, M. Buyuk, A. Suleman, et al., A hybrid damage assessment for E-and S-glass reinforced laminated composite structures under in-plane shear loading, Compos. Struct. 186 (2018) 347–354, https://doi.org/10.1016/j.compstruct.2017.12.023.

[33] C. Yilmaz, C. Akalin, I. Gunal, H. Celik, M. Buyuk, A. Suleman, et al., A hybrid damage assessment for E-and S-glass reinforced laminated composite structures under in-plane shear loading, Compos. Struct. 186 (2018) 347–354, https://doi.org/10.1016/J.COMPSTRUCT.2017.12.023.

[34] I. Emami Tabrizi, F.E. Oz, J. Seyyed Monfared Zanjani, S.K. Mandal, M. Yildiz, Failure sequence determination in sandwich structures using concurrent acoustic emission monitoring and postmortem thermography, Mech. Mater. 164 (2022) 104113, https://doi.org/10.1016/J.MECHMAT.2021.104113.

[35] F.E. Oz, N. Ersoy, S v Lomov, Do high frequency acoustic emission events always represent fibre failure in CFRP laminates? Compos. Appl. Sci. Manuf. 103 (2017) 230–235, https://doi.org/10.1016/J.COMPOSITESA.2017.10.013.